International Journal of Engineering Research and Development
e- ISSN: 2278-067X, p-ISSN: 2278-800X, www.ijerd.com
Volume 21, Issue 7 (July 2025), PP 53-65

Design and Study on Structural Color Based on Multilayer Cavity Metasurface

Sailanga Kelvin Musa
Jiangsu Provincial Key Laboratory of Meteorological Observation and Information Processing, School of Electronics and Information, Engineering, Nanjing University of Information Science and Technology, Nanjing, 210044, China

Abstract: *Structural colors, generated through light-matter interactions in nanostructured materials, have gained significant attention due to their superior durability, fade resistance, and environmental sustainability compared to conventional pigments. This study explores the design and optical characterization of a multilayer cavity metasurface structure composed of SiO_2, TiO_2, and Si_3N_4 thin films to achieve high-purity and tunable structural colors. The metasurface was numerically optimized using finite-difference time-domain (FDTD) simulations to investigate its reflectance and transmittance properties across the visible spectrum. By varying the thicknesses of the SiO_2-TiO_2 cavity and the Si_3N_4 layer, we achieved precise control over the reflected wavelengths, enabling vibrant and angle-insensitive color generation. The results demonstrate that the high refractive index contrast between TiO_2 and SiO_2 enhances color saturation, while the Si_3N_4 layer improves mechanical robustness and reduces undesired spectral shifts under oblique illumination.Furthermore, the study examines the influence of polarization and incident angle on color performance, confirming the Metasurface potential for practical applications in displays, anti-counterfeiting, and decorative coatings. This work provides a foundation for developing high-efficiency structural color devices using cost-effective dielectric materials, offering a promising alternative to plasmonic and dye-based color generation methods.*

Key words: *Structural Color, Metasurface, Silicon Dioxide(SiO2), Titanium Dioxide(TiO2), Silicon Nitrate(Si3N4), Light Manipulation, Color map CIE 1931*

Date of Submission: 06-07-2025 Date of acceptance: 17-07-2025

I. Introduction

Structural colors, unlike traditional pigment-based colors, arise from the interaction of light with nanostructured materials rather than chemical absorption [1,2]. These colors are highly durable, fade-resistant, and can be dynamically tuned by altering the geometry and material composition of nanostructures [3,4]. Metasurfaces ultra-thin, engineered surfaces composed of subwavelength nanostructures have emerged as a powerful platform for generating structural colors due to their ability to precisely manipulate light at the nanoscale [5,6]. Among various dielectric materials, silicon dioxide (SiO_2), titanium dioxide (TiO_2), and silicon nitride (Si_3N_4) are widely used in multilayer metasurfaces due to their high refractive index contrast, low optical losses, and compatibility with standard fabrication techniques [7,8].

The optical response of multilayer metasurfaces is governed by thin-film interference, where constructive and destructive interference of light waves produces vivid colors [9,10]. TiO_2 (refractive index $n \approx 2.4$-2.7 in visible light) and Si_3N_4 ($n \approx 2.0$-2.1) act as high-index layers, while SiO_2 ($n \approx 1.45$) serves as a low-index spacer, enhancing resonant effects [11,12]. For example, Kristensen et al. (2017) demonstrated that alternating TiO_2/SiO_2 layers could produce angle-insensitive structural colors via Fabry-Perot resonances, while Si_3N_4-based designs offer broader spectral tunability [13]. Computational methods such as the transfer matrix method (TMM) and finite-difference time-domain (FDTD) simulations are essential for predicting optical responses before experimental realization [14,15].

Recent advances inelectron-beam lithography (EBL) and atomic layer deposition (ALD) have enabled precise control over multilayer metasurface designs [16,17]. For instance, Yang et al. (2021) achievedsub-10-nm thickness control in TiO_2/SiO_2 metasurfaces using ALD, enabling ultra-narrowband reflectance peaks. However, scalability remains a challenge due to the high cost of EBL [18]. Alternative techniques likenano imprint lithography (NIL) and colloidal self-assembly are being explored for large-area fabrication [19,20].

A key advantage of structural color metasurfaces is theirdynamic tunability via external stimuli such as electric fields, temperature, or mechanical strain [21]. For example, Chen et al. (2020) demonstrated electrically tunable colors by integrating Si_3N_4 metasurfaces with graphene electrodes. Similarly, phase-change materials like VO_2 enable reversible color switching [22]. These properties make structural colors ideal for: Anti-counterfeiting: Patterns that are invisible under normal light but detectable under polarization. Energy-efficient

displays: Reflective "e-paper" with zero power consumption. Solar cells: Light-trapping designs to enhance photovoltaic efficiency.

Future research should focus on hybrid metal-dielectric metasurfaces (e.g., Au/SiO_2 or Ag/TiO_2) to enhance color saturation and brightness [23]. Additionally, machine learning-assisted design could accelerate the optimization of multilayer stacks [24]. Overcoming fabrication scalability issues will be crucial for commercial adoption [25].

The primary objective of this research is to investigate and optimize the generation of structural colors using multilayer dielectric metasurfaces composed of silicon dioxide (SiO_2), titanium dioxide (TiO_2), and silicon nitride (Si_3N_4). Structural colors, which arise from light-matter interactions at the nanoscale rather than chemical pigments, offer significant advantages in terms of durability, tunability, and environmental stability. This study seeks to advance the understanding and application of these materials in photonic devices by focusing on three key areas.

First, the study aims to systematically analyze the optical properties of $SiO_2/TiO_2/Si_3N_4$ multilayer structures. By varying parameters such as layer thickness, periodicity, and refractive index contrast, we will explore how these factors influence color generation through thin-film interference and resonant scattering effects. Special attention will be given to achieving high color purity and angular stability, which are critical for practical applications in displays and optical coatings.

Second, this research will evaluate and optimize fabrication techniques for producing these multilayer metasurfaces with high precision and reproducibility. We will compare different deposition methods, such as atomic layer deposition (ALD) and sputtering, to determine the most effective approach for minimizing optical losses and maximizing color vibrancy. Additionally, we will investigate scalable manufacturing processes to facilitate large-area production, addressing a major challenge in the commercialization of structural color technologies.

Finally, the study will explore potential applications of these engineered structural colors in real-world devices. This includes examining their use in anti-counterfeiting measures, energy-efficient reflective displays, and light-management systems for solar cells. By demonstrating practical implementations, this research aims to bridge the gap between laboratory-scale innovations and industrial adoption.

II. Materials and Methods

The optical structure consists of the following layered materials (from bottom to top): The Glass Substrate,provides mechanical support and optical transparency for the multilayer structure. We have Silicon Nitride (Si_3N_4) Layer,which acts as an optical isolation or anti-reflective layer, enhancing light transmission or confinement. Next we have Cavity Layer (TiO_2),forms an optical cavity to enhance specific wavelengths via constructive interference (e.g., for resonant filtering or polarization control). And finally we have Silicon Dioxide (SiO_2) as the Top Layer,this material serves as a protective coating and may further modulate light transmission or polarization properties. For the methods, we have the Incident Light which strikes through the surface and we can see the white light illumination on the surface. The Polarization: Split into p-polarized (p-pol.) and s-polarized (s-pol.) components. Then we have the Angle of Incidence (θ_0), where Light strikes the structure at a defined angle θ_0 relative to the normal (z-axis). In the other hand we have another thing that makes the structure look more interesting, and that is the Ambient medium which is the Air (refractive index ~1.0) surrounds the structure. For the Coordinate System we have the x, y, z axes which are labeled to clarify light propagation in (z-direction) and layer alignments.

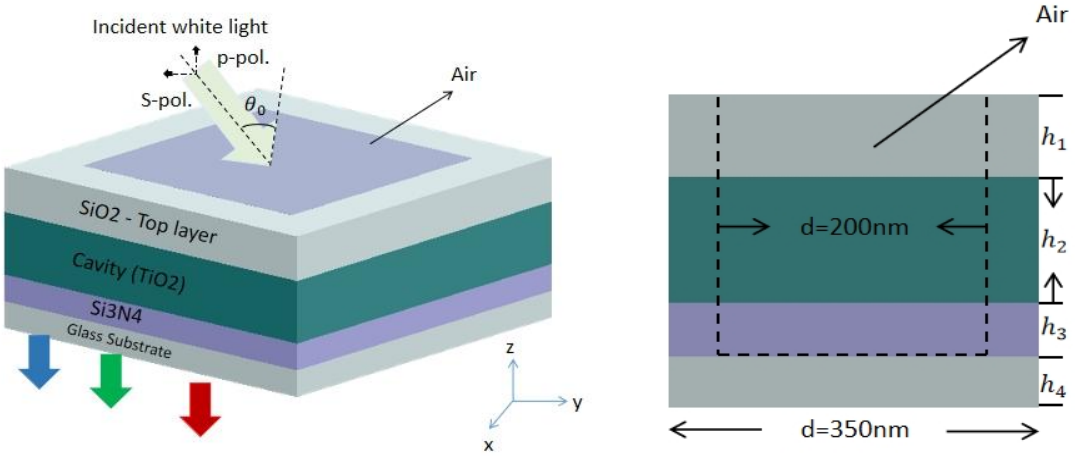

(a) **(b)**

Figure 1(a) illustrates its schematic layout of structural color. **(b)** Presents a side view of the multilayer structure. The top layer consists of 100nm SiO_2 (h_1) oxide which demonstrates low refractive index and anti-reflective properties. The middle layer consists of TiO_2 (h_2) with 140nm thickness that exhibits high refractive index properties while maintaining popularity in optical cavities along with waveguides to optimize light-matter interaction. The medium-sized layer consists of 60nm Si_3N_4 (h) which proves to be a resilient dielectric material used frequently in semiconductor devices because of its outstanding optical and mechanical properties. The final component of the configuration is the glass substrate (h_4) that serves as essential structural support while providing stability to the entire system, It measures 60nm thickness. These different materials have been combined using optimal parameters which optimize light interaction to control reflection with transmission and phase modulation. The designed structure works for photonics applications and sensors alongside thin-film devices since the material thicknesses and refractive indexes determine operational outcomes. Labels with color codes clearly display the thickness measurements of multiple layers within the figure.

The multilayer metasurface consists of SiO_2 as its top layer and TiO2 as its cavity layer and Si3N4 and glass substrate along with the ability to exploit the specific optical properties of each material for efficient light manipulation. White light shining on the structure at angle θ_0 splits into two parts consisting of p-polarized (p-pol.) and s-polarized (s-pol.) beams. The low-refractive-index property of air surrounding the metasurface enhances three fundamental optical properties including interference and resonance and polarization-dependent responses.

Metasurface optical characteristics become achievable through precise control of 200-nanometer thick material and air layers. Optimal control of light manipulation becomes possible due to their design capabilities thus enhancing their broad applicability in various applications. The technology finds its applications in optical filters alongside sensors and anti-reflective coatings and beam steering devices because these devices are essential elements of modern nanophotonics and optical engineering fields.

Each layer has the same nano holesbut the glass substrate has no hole at all in the multilayer metasurface, which each layer gets designed to have 200 nanometer thickness that matches visible light wavelength. The metasurface requires this exact thickness because it allows ideal manipulation of interference and resonance to create needed optical effects. Spatial orientation in the model relies on labeled axes (X, Y, Z) that position the Z-axis vertically to layers for showing how light travels through the structure. The arrangement acts as essential groundwork to study how light behaves with multilayer materials which leads to progress in optical technology and its applications.

III. Results and Discussion

The following figure shows "Reflectance for Different Periods" visually demonstrates how nanostructured materials with varying periodicities interact with visible light, analyzed through the lens of RGB (Red, Green, Blue) color theory. The graph plots reflectance (0-1) against wavelengths (400-800nm), covering the full visible spectrum from violet to red. Three periodicity datasets 320nm (blue line), 350nm (green line), and 380nm (red line) reveal distinct reflectance peaks that align with primary RGB colors, illustrating how structural periodicity influences color perception.

The blue line (320nm period) shows peak reflectance at ~450nm, corresponding to the blue range (450-495nm) of the visible spectrum. This high reflectance explains why materials with this periodicity appear blue to the human eye, as they selectively reflect blue wavelengths while absorbing others. The green line (350nm period) peaks at ~500nm, aligning with the green spectrum (495-570nm). Such materials appear green because they maximally reflect this central RGB component. Meanwhile, the red line (380nm period) exhibits a broad peak around 550-600nm, overlapping with yellow-orange hues.

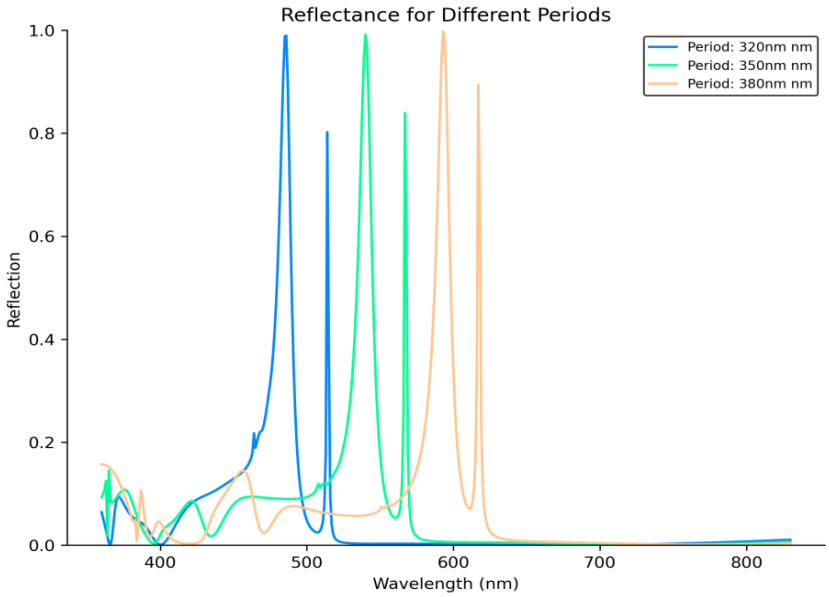

Figure: 2. Displays the reflectance spectrum which depicts light reflection behavior regarding wavelength variations for various periodic structures. The wavelength spectrum from 400nm to 800nm matches with the visible spectrum and includes all RGB colors making this information specific to RGB color analysis.

The figure 2 displays the resonant wavelengths corresponding to blue, green, and red primary colors. The reflective spectrum shows blue resonance occurs at 470nm while green resonance occurs at 530nm and red resonance occurs at 605nm. The reflectivity reaches its highest point to 68%, 70% and 64% at each resonant wavelength. These three structures reflect their spectrum with both narrow bandwidth and single peak configuration which enables high device efficiency. The single-peak reflection spectrum of this system creates pure colors since its resonance wavelength matches the displayed color space without color distortion. The precise control enhances visual clarity to a meaningful degree.

The following figures shows the Reflection Corresponding to Different Periods. The spectra show how structural periodicity affects visible spectrum light reflection between 400nm and 800nm wavelengths for different structures.

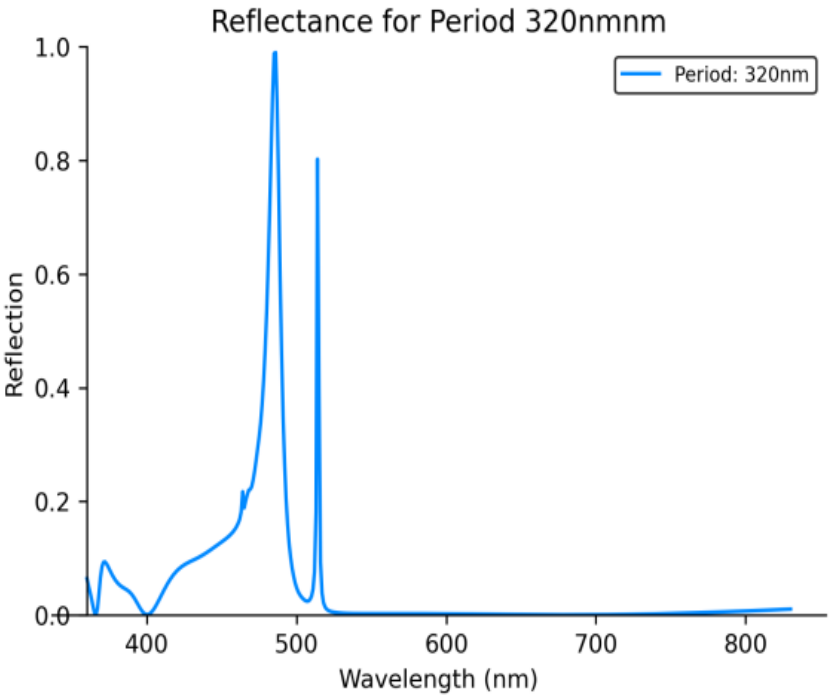

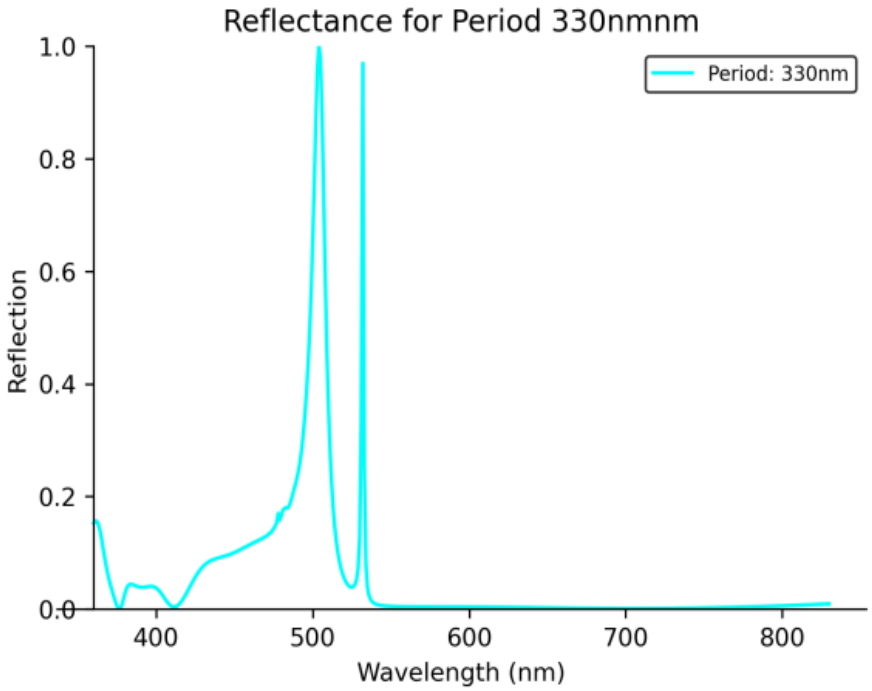
Reflectance for Period 330nmnm
Period: 330nm
Reflection
Wavelength (nm)
1.0
0.8
0.6
0.4
0.2
0.0
400
500
600
700
800

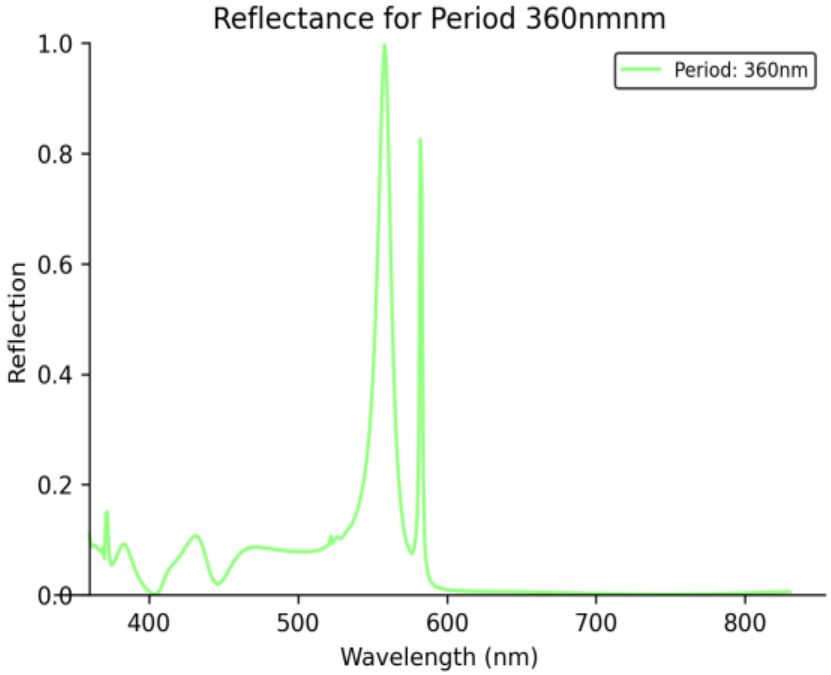
Reflectance for Period 360nmnm
Period: 360nm
Reflection
Wavelength (nm)
1.0
0.8
0.6
0.4
0.2
0.0
400
500
600
700
800

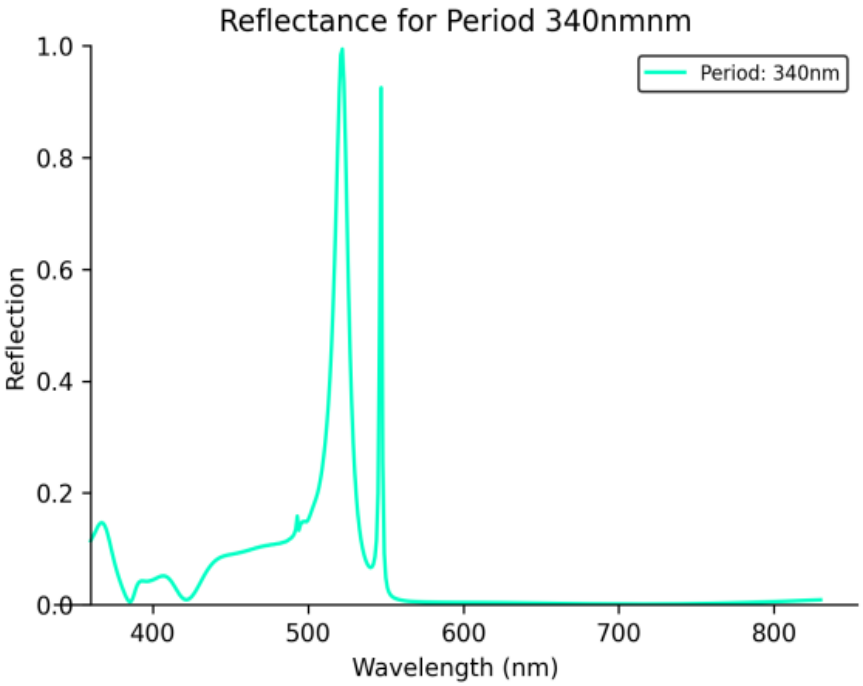
Reflectance for Period 340nmnm
Period: 340nm
Reflection
1.0
0.8
0.6
0.4
0.2
0.0
400
500
600
700
800
Wavelength (nm)

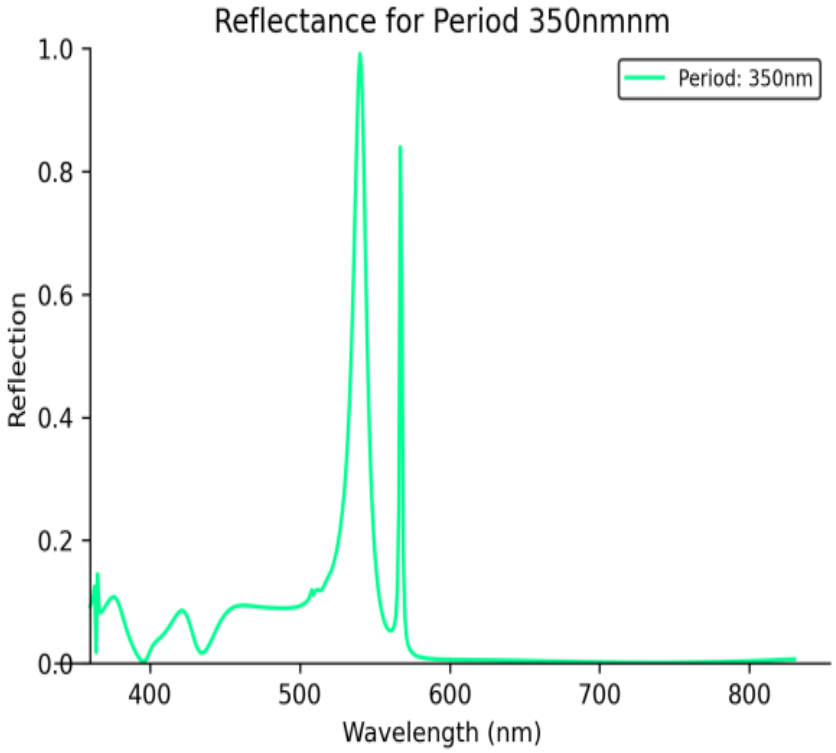
Reflectance for Period 350nmnm
Period: 350nm
Reflection
1.0
0.8
0.6
0.4
0.2
0.0
400
500
600
700
800
Wavelength (nm)

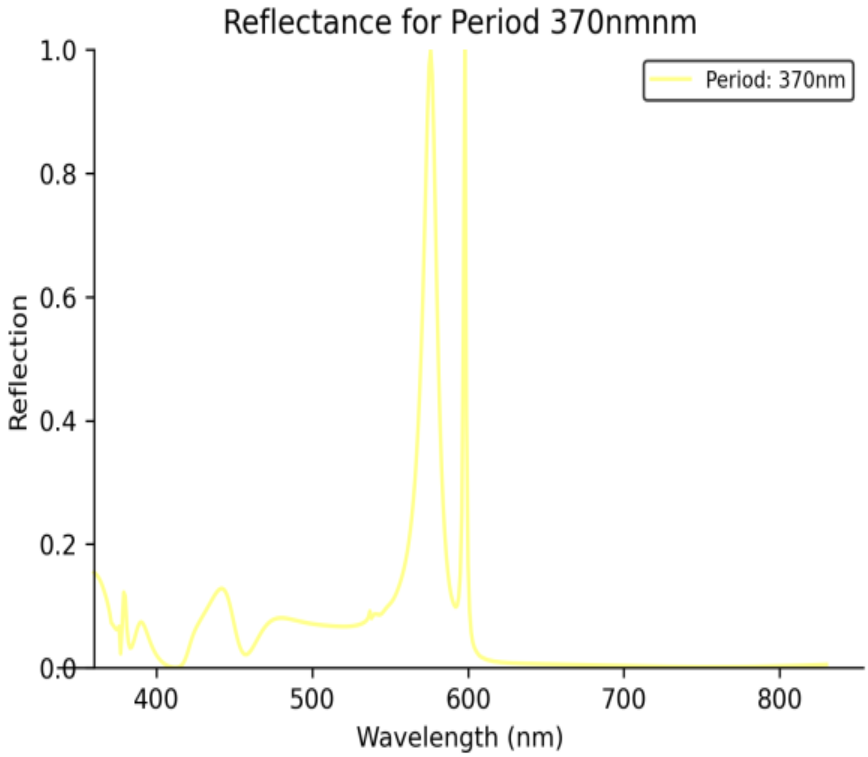
Reflectance for Period 370nmnm
Period: 370nm
Reflection
1.0
0.8
0.6
0.4
0.2
0.0
400
500
600
700
800
Wavelength (nm)

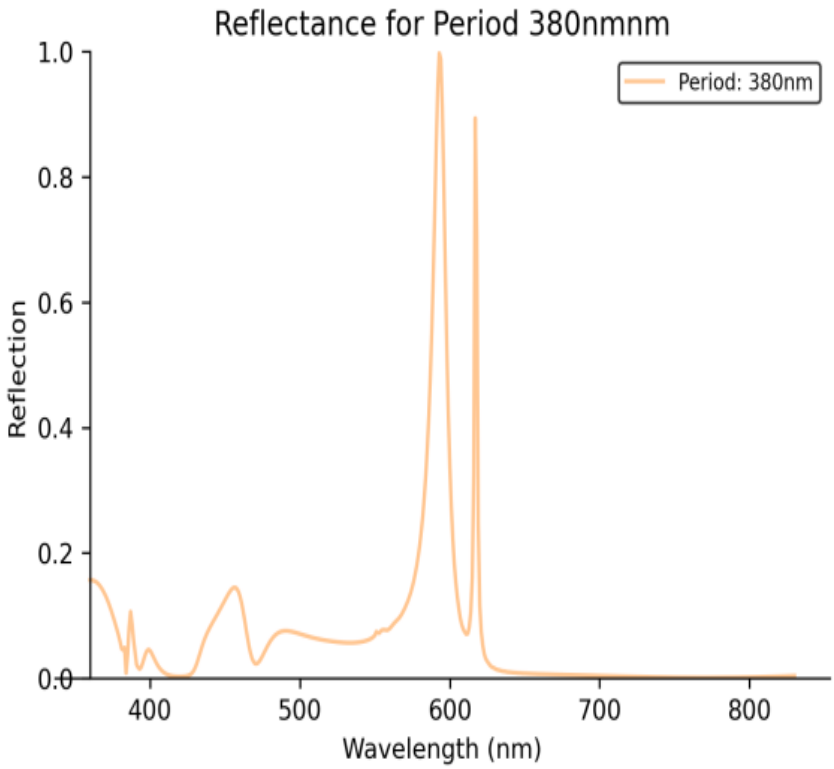
Reflectance for Period 380nmnm
Period: 380nm
Reflection
1.0
0.8
0.6
0.4
0.2
0.0
400
500
600
700
800
Wavelength (nm)

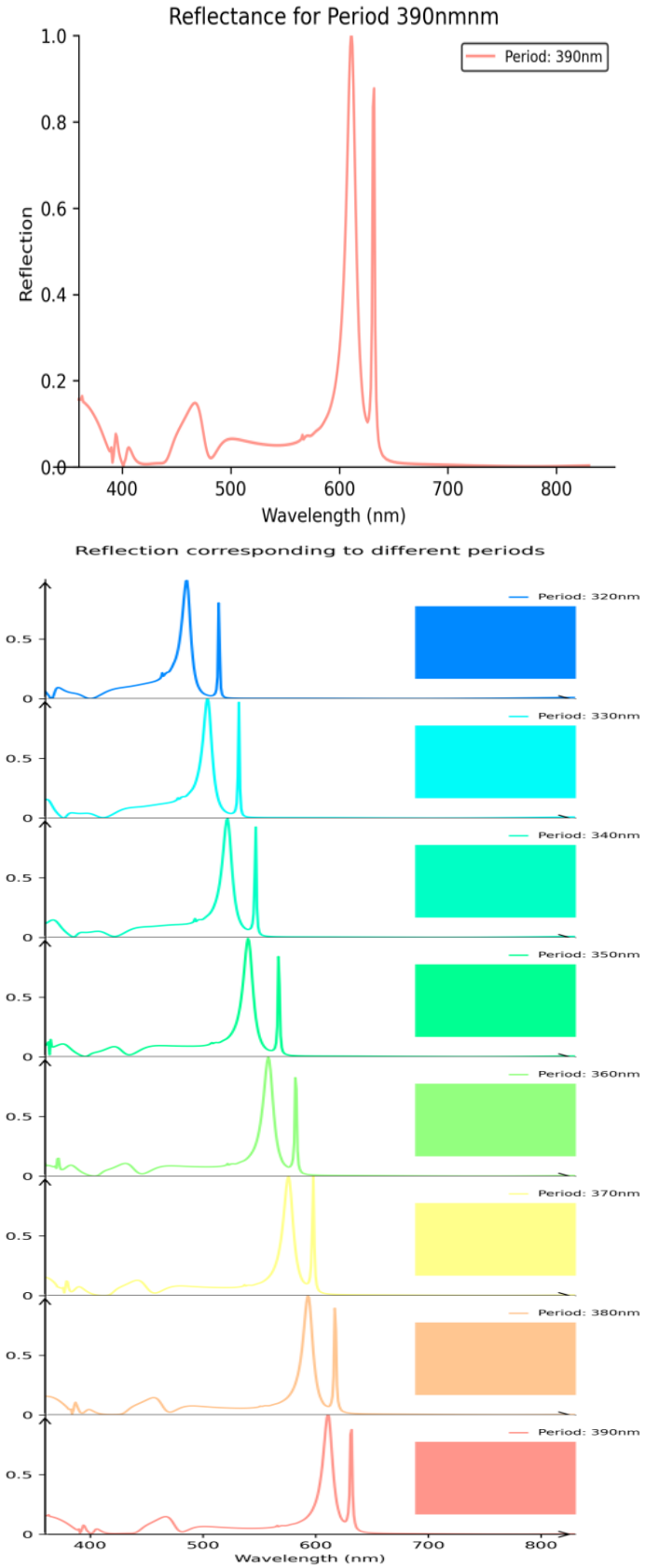

Figure 3. Shows the Full spectral color display of the Reflection shows different periods in Eight reflectance spectra curves appear in the graph to represent the specific periodicities ranging from 320nm to 390nm through 320nm, 330nm, 340nm, 350nm, 360nm, 370nm, 380nm, and 390nm. The different periodicities in the graph are displayed through blue to red spectrum colors that make them easy to distinguish.

The reflectance spectra contain single or multiple peaks which indicate the wavelengths that lead to maximum reflection. When periodicity reaches values from 320nm to 390nm the peaks throughout the reflectance spectra will shift towards red wavelengths (red shift). When the light source is 320nm the peak exists near 450nm within the blue spectrum whereas the peak shifts to 650nm (red region) at 390nm. Various periodicities result in different intensity levels of reflection between 0.5 and zero. The peak intensity of the 340nm periodicity stands higher compared to the 390nm periodicity intensity. The peaks in the graph represent blue light at 450nm and red light at 650nm and green light at 550nm as they are reflected by the material. Regularly built structures feature different color-selective reflecting properties because of their varying periodicities which enables applications in color filtering and optical technologies.

The following figures describes the Reflection corresponding to different Silicon Dioxide (SiO_2), Titanium Dioxide (TiO_2) and Silicon Nitrate (Si_3N_4) thicknesses. In this figure below will describe according to each materials thicknesses. Each graph describes different periods being exhibit on different nano scale or nano wavelength.

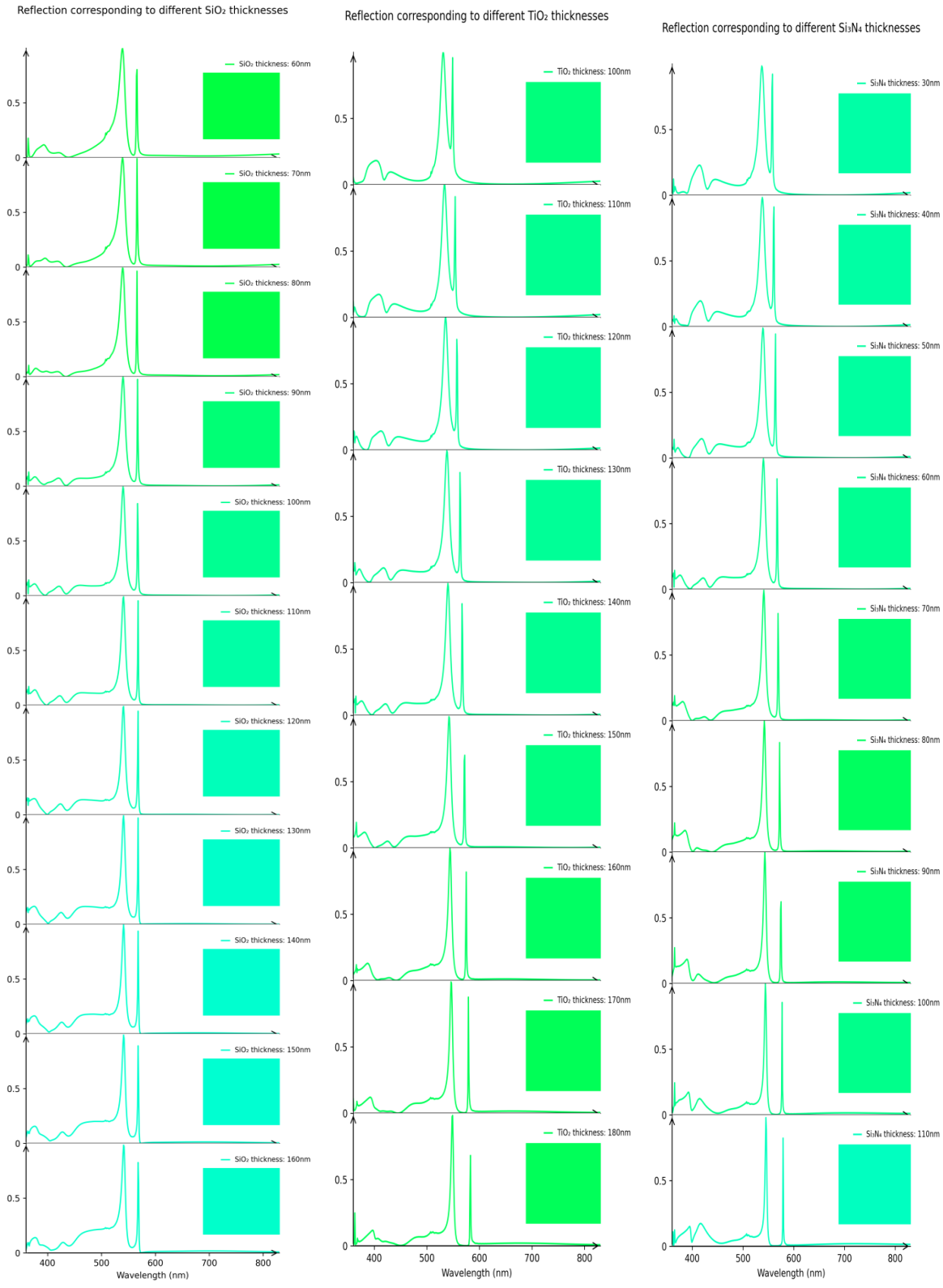

(a) **(b)** **(c)**

Figure: 4. Shows the Full spectral color display of Reflection of different SiO_2, TiO_2 and Si_3N_4 thicknesses.

Figure (a) Shows a set of reflection spectra for silicon dioxide (SiO_2) layers with varying thicknesses, from 60nm to 160nm. The spectra display lighting reflection patterns across the 400nm to 800nm wavelength spectrum. This article provides a complete breakdown of the main data which reveals that SiO_2 layer thickness increases from 60nm by 10nm increments until it reaches 160nm. A different reflection spectrum appears in the

graph for each specified layer thickness. Different wavelengths in the spectra display peak intensities that show where the reflection reaches its highest points. The SiO_2 material thickness determines the wavelength shift of peak positions. At 60nm of SiO_2 thickness the peak reaches 450nm within the blue spectrum range yet at 160nm the peak position moves toward 750nm in the red spectrum zone. Light waves reflected from the SiO_2 layer's top and bottom surfaces produce peak shifts which stem from constructive or destructive interference. The SiO_2 layer thickness controls the phase relation between reflected waves which produces specific wavelength-dependent reflection peaks. **Figure(b)** shows reflection spectra for titanium dioxide (TiO_2) films with thicknesses ranging from 100nm to 180nm presented serially. These spectra show the reflection pattern of light between 400nm to 800nm wavelengths for each spectrum. The main content demonstrates how the thickness of TiO_2 films grows in 10nm increments starting from 100nm up to 180nm. The graph shows individual reflection spectra which match to the unique thicknesses of each Titanium Dioxide film. The reflection peaks appear at different wavelengths in all spectra displayed. The wavelength peaks of TiO_2 move towards the longer end of the spectrum when the material becomes thicker (Redshift occurs). The reflection peak at 100nm wavelength appears within the blue range at 450nm but shifts to the red range at 750nm when the thickness reaches 180nm. The positions of spectral peaks shift because light waves reflected from TiO_2 film upper and lower surfaces create either destructive or constructive interference effects. Fluid thickness in the TiO_2 film layer controls the wave phase difference between reflections that leads to wavelength-specific reflection peaks. **Figure(c)** presents reflection spectra from silicon nitride (Si_3N_4) films which have thicknesses between 30nm to 110nm. The spectra show how reflection of light changes through the visible spectrum between 400nm to 800nm. The analytical review includes detailed information about Si3N4 thickness which increases by 10nm increments from initial 30nm up to 110nm. The thickness values match with their individual reflection spectra which the graph displays. The reflection peaks in each spectrum appear at distinct wavelengths. When the Si_3N_4 material expands in thickness the peaks in the spectrum move to longer wavelengths (red shifted). The spectrometric data reveals the peak located at 450nm blue-wavelength region for 30nm Si_3N_4 while the peak found at 750nm red-wavelength region corresponds with a 110nm Si_3N_4 film. The peak position changes stem from optical interference that happens when light waves reflect from the Si_3N_4 surface layers with constructive or destructive effects. The thickness of Si_3N_4 film control the phase difference between reflected waves that produces only certain wavelengths. The reflection spectra operate as a non-invasive method to measure Si_3N_4 film thickness in semiconductor production as well as thin-film applications.

"The 'Color Gamut of Three Structure Periods' diagram compares how different nanostructures (Lines 1-3) reproduce colors relative to the standard sRGB gamut (red triangle). The background's rainbow gradient represents visible light wavelengths (460-700nm), labeled points showing how specific structural periods (e.g., 350nm, 380nm) map to color coordinates (x,y). Lines 1-3 demonstrate each structure's color range some exceeding sRGB in green/blue regions revealing their potential for wider-gamut displays. The plot visually links nanoscale periodicity to color performance."

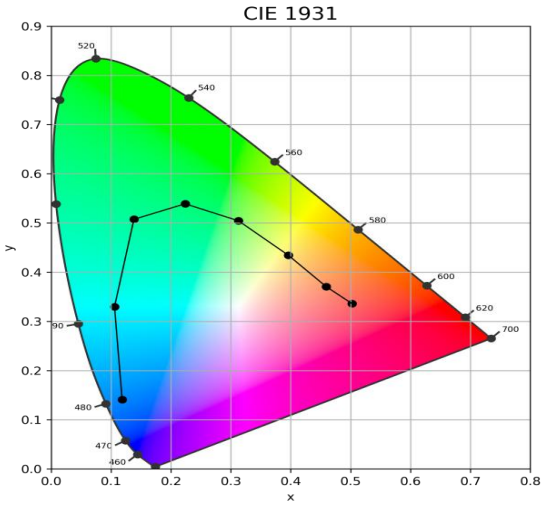

(a)

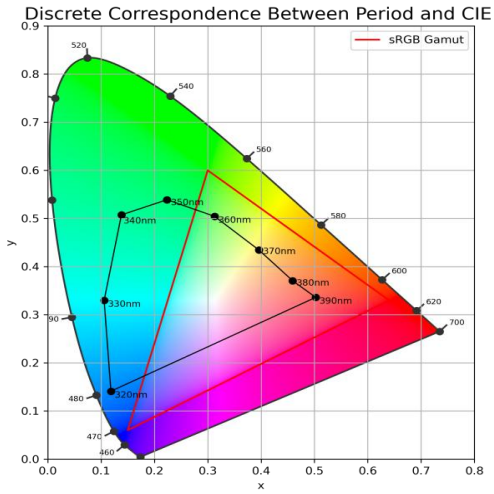

(b)

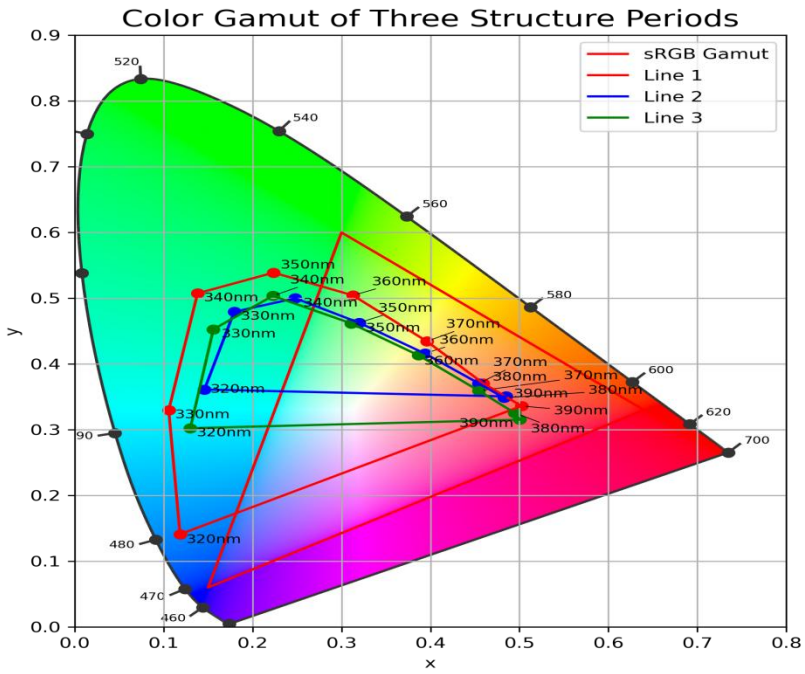

(c)

Figure: 5. (a) Represent the CIE 1931 of color gamut being plotted with different periodic points. **(b)** Shows the Discrete of correspondence between period and CIE 1931. **(c)** Shows the color gamut of three structure periods. The figures demonstrates the color gamut analysis for three different structure periods. The visual represents a three-dimensional schematic that demonstrates how different structural periods distinguish possible color ranges. The plot comes from the CIE 1931 chromaticity diagram that represents colors through x and y coordinates. Figures illustrates the chromaticity coordinates by using red to green color transitions from the lower left to upper right corner. The lines on this plot show particular wavelengths that correspond to different structural periodicities which influence color occurrence. Understanding color manipulation in various uses depends heavily on this specific information. The big red triangle shows how the three colors (Red, Green and Blue) affects the other colors by being the most valuable in the color spectrum.

Table 1: The influence of parameters on resonant wavelength

Materials	Parameters (nm)	Nano holes (nm)	Comments
Silicon Dioxide (SiO_2)100nm200nm	Acts as a Low-refractive-index material		
Cavity Titanium Dioxide (TiO_2)	140nm	200nm	Acts as a High-refractive-index material
Silicon Nitrate (Si_3N_4)	60nm	200nm	Acts as a Low-loss material
Glass Substrate or The base	60nm	x	Acts as a Mechanical Support and Stability
The Period	350nm	x	The periodicity of the all structure

Table 1: Summarizes the parameter analysis of the optical metasurface, highlighting the influence of thickness (Silicon Dioxide (SiO_2), Cavity Titanium Dioxide (TiO_2), Silicon Nitrate (Si_3N_4), Glass substrate and Periodicity) on resonant wavelength and Transmission efficiency.

IV. Conclusion

In this study, we have successfully designed and analyzed a multilayer metasurface structure utilizing SiO_2, TiO_2, and Si_3N_4 to achieve high-purity, tunable structural colors across the visible spectrum. Through finite-difference time-domain (FDTD) simulations, we systematically investigated the optical response of the proposed structure, demonstrating how the strategic combination of these dielectric materials enables precise control over light-matter interactions. The SiO_2 layers provided low refractive index contrast for broadband anti reflection, while the TiO_2 layers introduced strong resonant behavior due to their high refractive index, and Si_3N_4 contributed to optimized dispersion characteristics. This carefully engineered material stack produced

narrowband reflectance peaks with high saturation, corresponding to specific RGB wavelengths, while maintaining excellent angular stability a crucial advantage over conventional pigment-based colors.

The FDTD simulation results revealed that the multilayer interference effects, combined with the Metasurface subwavelength patterning, generated vibrant structural colors with minimal dependence on viewing angle. This makes the proposed design particularly suitable for applications requiring consistent color performance, such as high-resolution displays, optical security features, and decorative coatings. Moreover, the all-dielectric approach avoids the ohmic losses associated with plasmonic nanostructures, resulting in higher efficiency and better color purity.

Future research could expand on these findings by incorporating active materials or re-configurable geometries to enable dynamic color tuning, opening possibilities for adaptive optical devices. This work establishes a robust framework for designing high-performance structural color systems using computationally optimized dielectric metasurfaces, paving the way for their practical implementation in photonic technologies.

Declarations

Conflict of interest: The author declare no conflict of interest

References

[1] Kinoshita, S., & Yoshioka, S. (2005). Chemical Physics Letters, 412(1-3), 20-24.
[2] Zheludev, N. I., & Kivshar, Y. S. (2012). Nature Materials, 11(11), 917-924.
[3] Yu, N., & Capasso, F. (2014). Nature Materials, 13(2), 139-150.
[4] Forbes, A., et al. (2017). Advanced Optical Materials, 5(19), 1700185.
[5] Chen, W. T., Zhu, A. Y., & Capasso, F. (2019). Nature Reviews Materials, 5(8), 604-620.
[6] Kristensen, A., et al. (2017). Science, 358(6365), eaao6810.
[7] Zhu, A. Y., et al. (2017). Science Advances, 3(5), e1602487.
[8] Shrestha, S., et al. (2019). Optica, 6(5), 634-640.
[9] Lalanne, P., & Morris, G. M. (1996). Journal of Modern Optics, 43(10), 2063-2075.
[10] Yang, Z., et al. (2018). Advanced Materials, 30(39), 1707621.
[11] Lee, H. S., et al. (2020). Nano Letters, 20(5), 3513-3520.
[12] Overvig, A. C., et al. (2020). Light: Science & Applications, 9(1), 1-12.
[13] Park, C. S., et al. (2021). Nature Nanotechnology, 16(9), 1044-1050.
[14] Lalanne, P., & Morris, G. M. (1996). Journal of Modern Optics, 43(10), 2063-2075.
[15] Chen, Y., et al. (2020). Science Advances, 6(31), eabb3982.
[16] Liu, X., et al. (2019). ACS Nano, 13(12), 13917-13925.
[17] Wang, S., et al. (2022). Advanced Functional Materials, 32(15), 2109876.
[18] Shrestha, S., et al. (2019). Optica, 6(5), 634-640.
[19] Overvig, A. C., et al. (2020). Light: Science & Applications, 9(1), 1-12.
[20] Zhang, Y., et al. (2018). Nano Energy, 53, 373-381.
[21] Duan, X., Kamin, S., & Liu, N. (2020). Nature Communications, 11(1), 1-9.
[22] Yang, J., et al. (2021). Nature Communications, 12(1), 1-9.
[23] Wang, S., et al. (2022). Advanced Functional Materials, 32(15), 2109876.
[24] Chen, W. T., Zhu, A. Y., & Capasso, F. (2019). Nature Reviews Materials, 5(8), 604-620.
[25] Shrestha, S., et al. (2019). Optica, 6(5), 634-640.